Clays and Clay Minerals, Vol. 69, No. 3:328–338, 2021

EFFECT OF MONTMORILLONITE LAYER CHARGE ON THE THERMAL STABILITY OF BENTONITE

Yating Qin[1], Tongjiang Peng[1], Hongjuan Sun[1,*], Li Zeng[1], Yao Li[1], and Can Zhou[1]
[1] Key Laboratory of Solid Waste Treatment and Resource Recycle,
Southwest University of Science and Technology, Mianyang 621010, China

Abstract—The thermal stability of bentonite is vitally important for its application in the casting field and the layer charge of montmorillonite (Q_m) is one of its central crystal-chemical parameters. As the main component of bentonite, the influence of Q_m on montmorillonite properties and behavior needs to be considered if bentonite is to be used in high-temperature environments. The objective of the current study was to investigate the relationship between Q_m and the thermal stability of Chinese bentonite samples collected from Wuhu, Anhui Province (marked as WH); Xinyang, Henan Province (marked as XY); and Santai, Sichuan Province (marked as ST) below. The values of Q_m were obtained using the O (11) method, and the structural properties of the bentonite samples were characterized by X-ray diffraction (XRD), Fourier-transform infrared spectroscopy (FTIR), thermogravimetry-differential scanning calorimetry (TG-DSC), and field emission scanning electron microscopy (FESEM). The results showed that, in the samples investigated, Q_m was inversely related to the thermal stability of bentonite. The Q_m value (electrons per half unit cell, e/huc) was greatest for sample ST (0.725 e/huc), followed by sample XY (0.470 e/huc), and by sample WH (0.354 e/huc). The dehydroxylation temperature changed related to Q_m; the sample with the largest Q_m value was WH (701°C), followed by sample XY (684°C), and sample ST (630°C). After the samples were calcined at 600°C, sample WH had the best montmorillonite structural integrity with the greatest degree of reusability (78.21%); while the montmorillonite structures of samples XY and ST were destroyed, and their reusabilities were only 9.48 and 6.01%, respectively.

Keywords—Bentonite · Layer charge · Thermal stability · TG-DSC · Structure of montmorillonite

INTRODUCTION

Montmorillonite is the main component of bentonite, a dioctahedral layered silicate mineral composed of two sheets of silicon-oxygen tetrahedra and one sheet of aluminum (hydrogen) oxygen octahedra (Magzoub et al. 2017; Sun et al. 2015; Zhu et al. 2019). Montmorillonite has a series of unique properties (such as swelling, dispersibility, adsorption, and adhesion) because of its layer charge (Q_m) and the existence of hydrated cations between the layers (Caglar et al. 2016). Bentonite applications have been studied extensively, therefore, e.g. as a sorbent of organics and metals (Jiang et al. 2019), for catalyst support (Liu et al. 2020), as the main material in zeolite synthesis (Rakhimova et al. 2021), and as a binder for casting (Boylu, 2011; Gong et al. 2016).

Bentonite is highly plastic, and has good demolding capacity, excellent air permeability, and its physical and chemical properties are stable in high-temperature environments when it is used as a molding-sand binder in the foundry industry; metal castings rarely have defects such as sand inclusions and sand holes (Geng and Liu 2013; Jordan et al. 2013). When bentonite is used as a binder for casting wet sand molds, however, the main component of bentonite (i.e. montmorillonite) can be damaged because of the heating (Żymankowska-Kumon et al. 2012). This causes some of the bentonite to lose its bonding property and to become "burnt-out bentonite," further affecting the cycle times of the molding sand (Beňo et al. 2015). The thermal stability of bentonite is related mainly to the temperature at which montmorillonite loses an hydroxyl group (dehydroxylation). In high-temperature environments, the hydroxyl group is released from the octahedral sheet of the montmorillonite structure in the form of H_2O, which causes a gradual decline in the cohesive properties of the bentonite (Schnetzer et al. 2016). The temperature of montmorillonite dehydroxylation is generally 600–750°C (Bala et al. 2012). The main factors affecting this temperature are as follows: the substitutions of cations for Al^{3+} and Si^{4+} in the octahedral and tetrahedral sites, and structural Fe^{3+} decreases significantly the dehydroxylation temperature (Kaufhold et al. 2017; Wu et al. 2005); lattice defects or *cis*- and *trans*-structures (Wolters and Emmerich 2007); and the particle size (Gauglitz and Schwiete 1964). Currently, however, few reports detail the influence of Q_m on the thermal stability of montmorillonite.

In the crystal structure of montmorillonite, Si^{4+} in the tetrahedral sheet can be substituted by Al^{3+} and Fe^{3+}, while Al^{3+} and Fe^{3+} in the octahedral sheet can be replaced by Mg^{2+} and Fe^{2+}; thus, the layer becomes negatively charged (Finck et al. 2019; Qiu et al. 2007, 2019a, b), i.e. Q_m. To balance these negative charges, montmorillonite adsorbs cations from the surrounding environment, which complicates the chemical composition of montmorillonite (Yang et al. 2019). The size of Q_m varies with the cause and place of origin of

* E-mail address of corresponding author: sunhongjuan@swust.edu.cn
DOI: 10.1007/s42860-021-00117-w

Table 1 Chemical composition (wt.%) of bentonite in the various samples examined

Samples	SiO_2	Al_2O_3	MgO	CaO	Fe_2O_3	K_2O	Na_2O	TiO_2	L.O.I
WH	71.69	13.78	1.22	1.94	1.56	0.28	0.51	0.17	8.57
XY	73.22	11.75	2.57	1.39	0.89	0.16	0.26	0.11	9.38
ST	59.28	16.01	4.58	2.41	2.59	1.14	0.17	0.28	13.34

montmorillonite. Q_m is a very important crystal chemical property of montmorillonite, which exerts a critical influence over many other properties of the montmorillonite (Qiu et al. 2007; Sans et al. 2017; Chen et al. 2018; Yang et al. 2019; Koutsopoulou et al. 2020). For example, Q_m can affect the hydration (Qiu et al. 2019a, b), exfoliation (Chen et al. 2018), and adsorption properties (Qiu et al. 2019a, b) of bentonite.

The objectives of the present study were to investigate the influence of Q_m on the thermal stability of montmorillonite, using the O (11) method to calculate the Q_m of each sample, and to determine the relationship between Q_m and the reusability of bentonite.

MATERIALS AND METHODS

Materials

The bentonite samples (<0.075 mm size fraction) used in the present study were collected from Wuhu, Anhui Province; Xinyang, Henan Province; and Santai, Sichuan Province, China. The main chemical components (Table 1) in the bentonite samples were SiO_2 and Al_2O_3, with minor amounts of MgO, CaO, Na_2O, Fe_2O_3, and K_2O, etc. The SiO_2 contents of sample XY and sample WH were relatively high, exceeding 70% in both, while that of sample ST was least at 59.52%. Anhydrous sodium pyrophosphate was supplied by Chengdu Kelong Co., Ltd., Chengdu, China, (AR).

Experimental Investigation

Purification treatment. 20 g samples of WH, XY, and ST bentonites were weighed, and the solid:liquid ratio was 1:20 (m:v). Anhydrous sodium pyrophosphate (0.3%) was added and the solution was stirred with a high-speed homogeneous mixer (FJ300-SH, Shanghai specimen model factory, Shanghai, China) for 50 min. Then, the mixture was separated using a centrifuge (F-34–6-38, Eppendorf Centrifuge 5804 R, Eppendorf AG, Hamburg, Germany) operated at 2000 rpm ($581.36\times g$) for 2 min; the upper suspension was sonicated for 10 min, and was centrifuged again at 5000 rpm ($3633.50\times g$) for 3 min. The lower suspension was dried at 105°C, ground, and stored in bags. The samples were marked as WH-T, XY-T, and ST-T.

Layer-charge calculation. Semi-quantitative analysis was performed on samples WH-G, XY-G, and ST-G; then, the components were normalized to obtain the percentage of each component (Table 2) (Kaufhold et al. 2003; Ufer et al. 2008). The O (11) calculation method (Sun et al. 2007) was used to calculate the structural formula of montmorillonite in the bentonite samples for each mining area. That is, according to the principle of balance of total negative and positive charges in the structural formula of montmorillonite: the mass percentage of each chemical component in the samples was converted to atomic number and the total valence of cations in the interlayer domain is the montmorillonite Q_m. Then, the Q_m value (e/huc) was calculated from the crystal-chemical formula of each montmorillonite (Table 3).

Calcination treatment. A box-type furnace (KSD-6-1300, Mianyang Jinguan Technology Co., Ltd., Mianyang, China) was heated to 600°C and kept at this temperature for 60 min. Then, 5 g of each bentonite sample was placed in porcelain crucibles and placed in the pre-heated box-type furnace. Timing started when the furnace temperature reached the set temperature. Samples were then cooled to room temperature, ground, and stored in bags. Samples were marked as WH-600, XY-600, and ST-600.

Determination of methylene blue consumption. The dried bentonite sample (0.2 g) was rewetted by adding it to a 250 mL conical flask with 50 mL of distilled water. Then,

Table 2 Chemical composition (wt.%) of bentonite in the various samples examined after purification and normalization

Samples	SiO_2	Al_2O_3	MgO	CaO	Fe_2O_3	K_2O	Na_2O	TiO_2
WH-T	66.17	23.17	2.50	2.51	2.60	1.61	0.16	0.19
XY-T	66.88	22.32	5.13	2.37	1.26	0.33	0.92	0.18
ST-T	62.99	22.64	7.00	3.30	2.71	0.53	0.18	0.27

https://doi.org/10.1007/s42860-021-00117-w Published online by Cambridge University Press

Table 3 Structural formula and Q_m of montmorillonite samples calculated by the O (11) method

Sample	Structural formula of montmorillonite	Q_m (e/huc)
WH-T	$(Ca_{0.078}Na_{0.186}K_{0.012})_{0.276}(H_2O)_n\{(Al_{1.570}Mg_{0.222}Fe^{3+}{}_{0.117}Ti^{4+}{}_{0.009}Ca_{0.082})_{2.000}[(Si_{3.943}Al_{0.057})_{4.000}O_{10}(OH)_2]\}$	0.354
XY-T	$(Ca_{0.150}Na_{0.105}K_{0.025}Mg_{0.020})_{0.300}(H_2O)_n\{(Al_{1.505}Mg_{0.431}Fe^{3+}{}_{0.056}Ti^{4+}{}_{0.008})_{2.000}[(Si_{3.951}Al_{0.049})_{4.000}O_{10}(OH)_2]\}$	0.470
ST-T	$(Ca_{0.211}Na_{0.021}K_{0.040}Mg_{0.121})_{0.393}(H_2O)_n\{(Al_{1.363}Mg_{0.503}Fe^{3+}{}_{0.122}Ti^{4+}{}_{0.012})_{2.000}[(Si_{3.767}Al_{0.233})_{4.000}O_{10}(OH)_2]\}$	0.725

20 mL of sodium pyrophosphate solution (1%) was added, the mixture was shaken and boiled on an electric stove for 5 min, followed by cooling to room temperature in air. A burette was used to drip methylene blue solution into the sample solution under constant shaking to achieve full reaction. Then, a drop of the test solution was dropped, using a glass rod, onto medium-speed, quantitative filter paper to check whether a pale blue halo appeared around the dark blue spot. If it did not appear, methylene blue solution was added dropwise until a light blue halo was observed on the filter paper, which marked the end point of the titration and the relevant titration volume. The methylene blue consumption of bentonite was calculated according to formula 1:

$$MB = \frac{cV}{m} \times 100 \quad (1)$$

where the MB (g/100 g) represents the consumption of methylene blue; c (g/mL) represents the concentration of methylene blue solution; V (mL) represents the titer of methylene blue solution; m (g) represents the bentonite mass; and 100 is the coefficient of the amount of methylene blue consumption of 1 g of bentonite converted to 100 g of bentonite. The arithmetic mean of the parallel determination results was taken as the measurement result, and the relative deviation between the two parallel determinations did not exceed 2%.

Swelling value test. A dried bentonite sample (3 g) was added to a measuring cylinder containing 50–60 mL of distilled water. The stopper was inserted tightly and the mixture was shaken until even dispersion was achieved. Then, 5 mL of ammonium chloride solution was added, and distilled water was added continually to the 100 mL graduation line. After shaking for 1 min, and allowing the mixture to settle for 24 h, the scale value of the precipitate interface was read. The arithmetic mean of parallel results was taken as the measurement result, and the absolute error of the two parallel determinations did not exceed 2 mL.

Reusability test. The box-type furnace was again heated to 600°C and kept at this temperature for 60 min. Then 5 g bentonite samples in porcelain crucibles were placed in the pre-heated furnace. Timing started when the furnace temperature reached the pre-set temperature. After heating for 60 min, the samples were cooled to room temperature. Then, the methylene blue consumption of bentonite after calcination was measured according to the test method (above) for the determination of the amount of methylene blue consumption. The reusability of bentonite was calculated according to formula 2:

$$F_B = \frac{MB_1}{MB} \times 100 \quad (2)$$

where F_B (%) represents reusability; MB_1 (g/100 g) represents the methylene blue consumption of bentonite after calcination at 600°C; and MB (g/100 g) represents the amount of methylene blue consumed by bentonite before calcination at 600°C.

Characterizations of both composition and structure. The chemical composition of the samples was assessed using a Panax Axios X-ray fluorescence spectrometer (XRF, PANalytical B.V., Eindhoven, The Netherlands) with a ceramic X-ray tube (Rh target), and a maximum power of 2.4 kW. The phase and structural characteristics of the samples were studied by X'Pert MPD Pro X-ray diffraction (XRD, PANalytical B.V., Eindhoven, The Netherlands) with Cu target at 40 kV and 40 mA, and a scanning range of 3–80°2θ. Changes in molecular vibrational spectra of the samples were characterized using FTIR on a Nicolet-5700 infrared spectrometer (Perkin Elmer, Waltham, Massachusetts, USA). The wavenumber range was 400–4000 cm^{-1}, and the KBr pellet technique was used. Changes in the thermogravimetric and differential scanning calorimetry (DSC) of samples were measured using an SDT Q600 synchronous thermal analyzer (TG-DSC, TA Instruments, New Castle, Delaware, USA). The heating rate was 20°C/min, in air atmosphere, and the air-flow rate was 100 mL/min. The micromorphology of the samples was analyzed using a Carl Zeiss Sigma300 field emission scanning electron microscope (SEM, Carl Zeiss NTS GmbH, Oberkochen, Germany).

Performance characterization. The methylene blue consumption, swelling value, and reusability of samples were measured according to the Chinese Industry standard JBT 9227–2013 'Bentonite for Foundry' (National Foundry Standardization Technical Committee 2013).

https://doi.org/10.1007/s42860-021-00117-w Published online by Cambridge University Press

RESULTS AND DISCUSSION

Phase Composition of Bentonite Samples

The characteristic reflections (001) of montmorillonite in the bentonite from the three mines all exceeded 1.50 nm (Fig. 1). The d_{001} value of montmorillonite is related to the type of interlayer cation and the thickness of the adsorbed water layer. If Ca^{2+} is the interlayer cation, the water molecular layer consists of two layers with a basal spacing of 1.40–1.55 nm. If the interlayer cation is Na^{+}, the water molecular layer consists of a single layer with a basal spacing of 1.20–1.25 nm. The d_{001} values of montmorillonite in samples WH, XY, and ST were 1.5337 nm, 1.5180 nm, and 1.5196 nm, respectively, which meant that all three bentonite samples were Ca-bentonite. The impurities contained in sample WH were mainly cristobalite and quartz; the impurities contained in sample XY were mainly cristobalite; and the impurities contained in sample ST were mainly quartz. The cristobalite content was greatest in sample WH and the quartz content was greatest in sample ST.

Dynamic Thermal Effect Changes

As shown by the TG-DSC curves of different bentonite samples (Fig. 2), all three samples had three endothermic effects on the DSC curves near the temperatures of 90–110, 630–701, and 888–969°C. These were caused by the endothermic processes of montmorillonite stripping off adsorbed and interlayer water (Grim and Rowland 1942; Boeva et al. 2016), as well as the decomposition and destruction of the layer structure (Alver and Gunal 2016). Two distinct weightless phases were visible on the TG curve, which correspond to the endothermic effect of the removal of

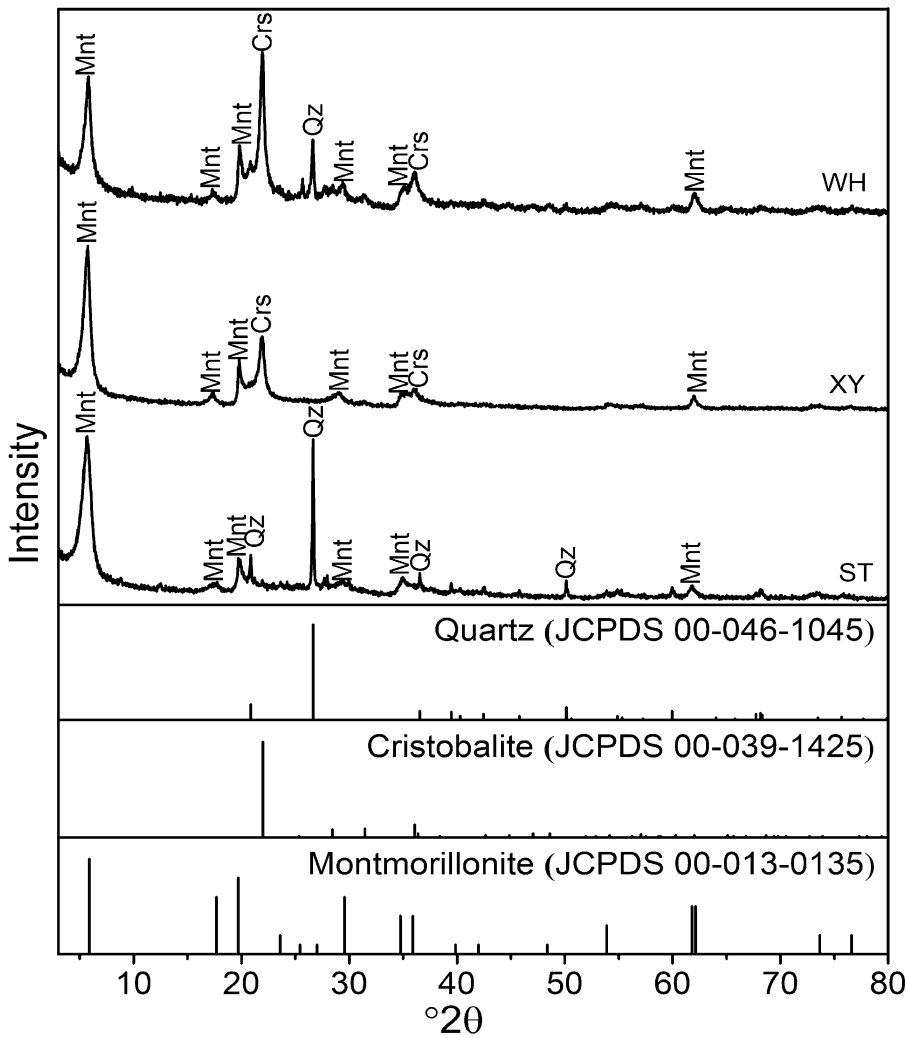

Fig. 1 XRD patterns of the bentonite samples

https://doi.org/10.1007/s42860-021-00117-w Published online by Cambridge University Press

Table 4 Analytical data for the dynamic thermal effects of bentonite samples

Samples	Dehydration temperature (°C)		Mass loss caused by dehydration (%)	Dehydroxylation temperature (°C)	Mass loss caused by dehydroxylation (%)	Total mass loss (%)
	I	II				
WH	96	171	9.21	701	4.40	13.61
XY	105	175	11.74	684	4.74	16.48
ST	109	175	12.60	630	5.17	17.77

interlayer and structural water on the DSC curve. The total weight losses of WH, XY, and ST samples were 13.61, 16.48, and 17.77%, respectively (Table 4). Because the quartz and cristobalite present in the samples did not lose weight during heating, the total weight loss represented the relative extent of the montmorillonite content in the samples. This indicated that the amount of impurities was greatest in sample WH, average in sample XY, and least in sample ST, consistent with the XRD results.

The three samples had weak adsorption peaks (at 171 and 175°C), toward the high-temperature end of the temperature range 95–175°C. This was related to the fact that the exchangeable cation in the interlayer domain of montmorillonite was mainly Ca^{2+}. Because two water layers were present in the interlayer and the hydration energy of Ca^{2+} was large, the adsorbed water was lost first; then the water coordinated to Ca^{2+} was lost, thus accounting for peaks near 171 and 175°C. As the hydration energy of Na^{+} is smaller than for Ca^{2+}, the dehydration temperature of the adsorption shoulder of sample WH was lower because of the relatively high Na_2O content. The temperature of the endothermic valley generated by the dehydroxylation of montmorillonite and the decomposition of the structural layer are important indicators of the thermal stability of montmorillonite (Alver and Gunal, 2016; Wu et al. 2005). In other words, the greater the temperature of transitions in the DSC patterns, the better the thermal stability of montmorillonite. The temperatures of the endothermic valley of the three samples showed obvious regularity, i.e. these temperatures increased with decreasing Q_m (Table 3). The Q_m of sample ST was greatest at 0.725 e/huc, and the temperatures at which dehydroxylation and structural-layer decomposition occurred were least (630 and 888°C, respectively); the Q_m of sample XY was in the middle at 0.470 e/huc, and the temperatures at which dehydroxylation and structural-layer decomposition occurred were greater (centered at 684 and 915°C, respectively); the Q_m of sample WH was least at 0.354 e/huc, and the temperatures at which dehydroxylation and structural-layer decomposition occurred were greatest (centered at 701 and 969°C, respectively). The dynamic thermal stability of montmorillonite decreased with increasing Q_m.

Changes in Samples after Static Heating

Compared with the original samples, the diffraction peaks of quartz and cristobalite in the samples calcined at 600°C for 60 min did not change significantly (Fig. 3). The characteristic peak (001) of montmorillonite disappeared, however, and a new, weak diffraction peak with d = 0.95–0.97 nm appeared. According to the thermal effect change of montmorillonite (Fig. 2), the interlayer water of montmorillonite in all samples was lost after calcination at 600°C, but the layered structure was retained. Because of the loss of water between the layers, the largest basal spacing decreased and became an illite-like structure. Because of the loss of interlayer water and the corresponding adjustment of structural layering, the disorder of layer stacking increased, while the peak intensity of the largest basal spacing decreased. The largest basal spacings of samples WH-600, XY-600, and ST-600 were 0.9613, 0.9540, and 0.9758 nm, respectively, which were related to the amounts of CaO and Na_2O in the original samples. Because the Ca^{2+} hydrated radius exceeded that of Na^{+}, sample ST-600 (with the greatest CaO content in the original sample) had the largest basal spacing, which was followed by sample WH-600, and then by sample XY-600 with the smallest value.

Changes in Vibrational Spectra

The characteristic bands of the FTIR spectra of different bentonite samples clearly identified montmorillonite in the samples (Fig. 4, Table 5) (Holtzer et al. 2011; Paluszkiewicz et al. 2008; Żymankowska-Kumon et al. 2012). The structural hydroxyl stretching band appeared at 3624–3633 cm^{-1}, and the band at 1638–1642 cm^{-1} represented the bending band of adsorbed H_2O (Hoang-Minh et al. 2019; Sakizci et al. 2010). The bands in the three samples at 1035–1103 cm^{-1} were different. Samples WH and XY had two absorption bands, while sample ST had only one. The reason for this may be that when the amount of Ca^{2+} in the interlayer was large, the strong hydration of Ca^{2+} allowed the hydrogen atoms from the Ca^{2+}-coordinated H_2O to form a stronger hydrogen bond with basal oxygens, causing band #4 (Fig. 4) of Si-O to shift to a lower wavenumber and/or become infrared inactive (Wu et al. 1999). Sample ST contained more Ca^{2+} than the other two samples (Table 1). After the samples

https://doi.org/10.1007/s42860-021-00117-w Published online by Cambridge University Press

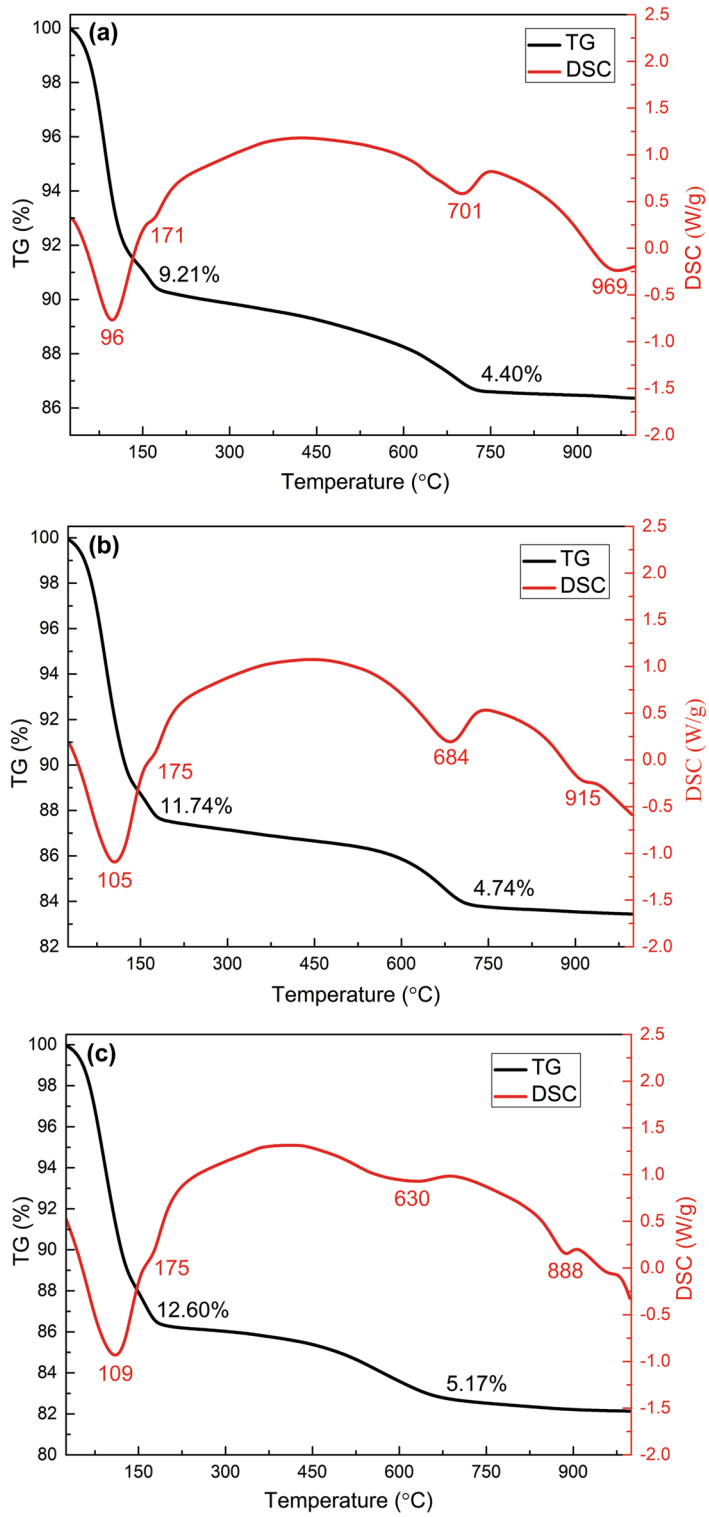

Fig. 2 TG-DSC patterns of bentonite samples: **a** WH, **b** XY, and **c** ST

https://doi.org/10.1007/s42860-021-00117-w Published online by Cambridge University Press

were calcined at 600°C, no obvious changes were found in the absorption bands at 1035–1103 cm^{-1}. The absorption bands of the three samples at 3624–3633, 1638–1642, 914–923, and 519–523 cm^{-1} all decreased significantly or even disappeared. Combined with the above analysis of the thermal effect on montmorillonite, the reason may be that montmorillonite started the dehydroxylation reaction under high temperature, which weakened the absorption band of hydroxyl groups. In addition, the dehydroxylation of montmorillonite caused the fracture of Al–Al–OH in the structure, which led to the disappearance of the characteristic absorption band (Holtzer et al. 2011; Paluszkiewicz et al. 2008). The weaker the absorption band, the worse the thermal stability of bentonite. The absorption bands at 3633 and 1639 cm^{-1} of sample ST with the highest Q_m were weakened the most (Fig. 4), which also indicated that the montmorillonite in sample ST was damaged to the greatest extent.

Microstructural Change

The montmorillonite layers in bentonite ore were complete and the pore structure between the layers was obvious (Fig. 5a, b, c). The layers of the calcined samples

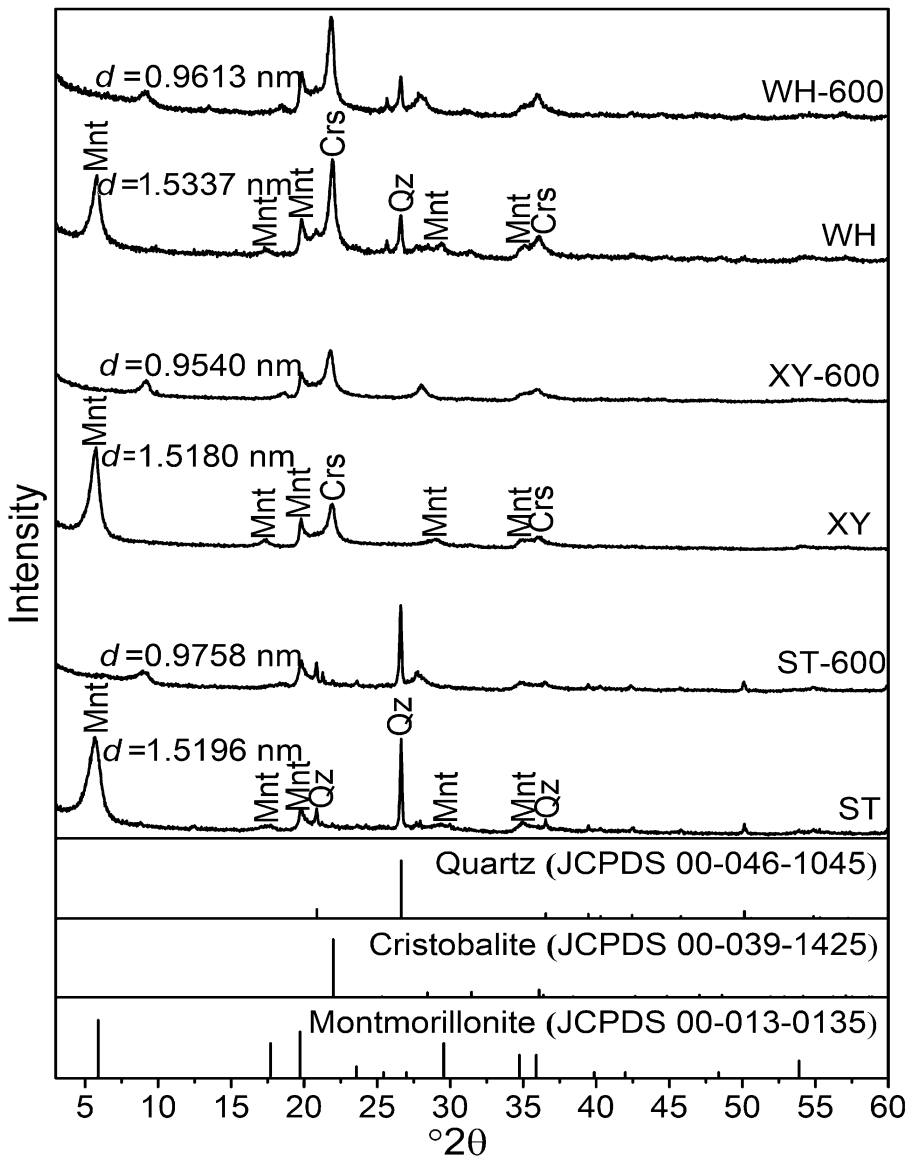

Fig. 3 XRD patterns of the bentonite samples before and after calcination at 600°C

https://doi.org/10.1007/s42860-021-00117-w Published online by Cambridge University Press

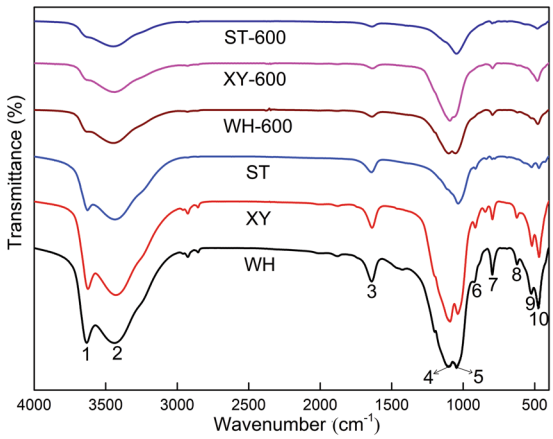

Fig. 4 FTIR patterns of the bentonite samples before and after calcination at 600°C (see Table 5 for assignments of the numbered bands)

were damaged to varying degrees, and partial melting had occurred (Fig. 5d, e, f). In addition, the pore structure was blocked because the layers had collapsed and were stacked on top of each other. This can be attributed to the dehydroxylation of montmorillonite (caused by high-temperature treatment), which resulted in defects in the crystal structure, and the collapsing of layers blocked pore channels (Sarikaya et al. 2000; Yang et al. 2006). Comparison of the images of each sample before and after calcination showed that sample ST was damaged the most, indicating further that the thermal stability of sample ST was the worst among the three samples.

Performance Change and Underlying Mechanism

The swelling values of samples WH, XY, and ST decreased in sequence; the consumption of methylene blue by the samples (after calcination at 600°C) decreased in turn; and the reusability also decreased in the same sequence (Table 6). Related to the Q_m of samples (Table 3), the swelling of bentonite may be concluded to decrease as Q_m decreases; the consumption of methylene blue after calcination increases with decreasing Q_m, and the reusability decreases with increasing Q_m. The Q_m in sample WH was least but had the highest level of reusability (78.21%), which was followed by samples XY (9.48%) and ST (6.01%).

The chemical composition and the phase-composition characteristics of the bentonite samples, as well as the thermal effects on montmorillonite and the change in the structure and FTIR absorption spectra of the calcinated samples, showed that the reusability of bentonite depended mainly on the thermal stability of montmorillonite. The thermal stability of montmorillonite, in turn, depended on the Q_m. One concludes, therefore, that the reusability of bentonite depends on Q_m. The reusability of bentonite increased with decreasing Q_m. The high-temperature stability of bentonite (including the reusability) may have been affected by Q_m because the generation and extent of Q_m was related to the the substitutions of cations for Al^{3+} and Si^{4+} in the octahedral and tetrahedral sites. When the amount of Al^{3+} substitution in montmorillonite was large, resulting in a greater Q_m, the structural stability of montmorillonite was reduced (Chai et al. 2013). During the heat treatment, the temperature at which the structure of montmorillonite was destroyed decreased, thus affecting the reusability of bentonite. In contrast, when the amount of substitution for Al^{3+} was small, Q_m was small, the stability improved, and the thermal stability was also

Table 5 Assignment of infrared absorption bands (cm^{-1}) of bentonite samples before and after calcination at 600°C (see Fig. 4). υ = stretching mode, δ = bending mode

Spectral peak number	WH	XY	ST	WH-600	XY-600	ST-600	Assignment
1	3633	3624	3628	3631	3627	3628	υ-OH
2	3437	3430	3437	3445	3436	3447	υ-H_2O
3	1639	1638	1642	1639	1637	1638	δ-H_2O
4	1103	1091		1100	1092		υ-Si–O
5	1047	1039	1035	1052	1048	1047	υ-Si–O-Si
6	923	916	914				δ-Al-Al–OH
7	797	796	798	796	795	798	δ-Mg–Al-OH
8	623	625		621	620		δ-Si–O-Al
9	523	519	522				δ-Si–O-Mg
10	475	471	471	479	482	482	δ-Si–O-Fe

https://doi.org/10.1007/s42860-021-00117-w Published online by Cambridge University Press

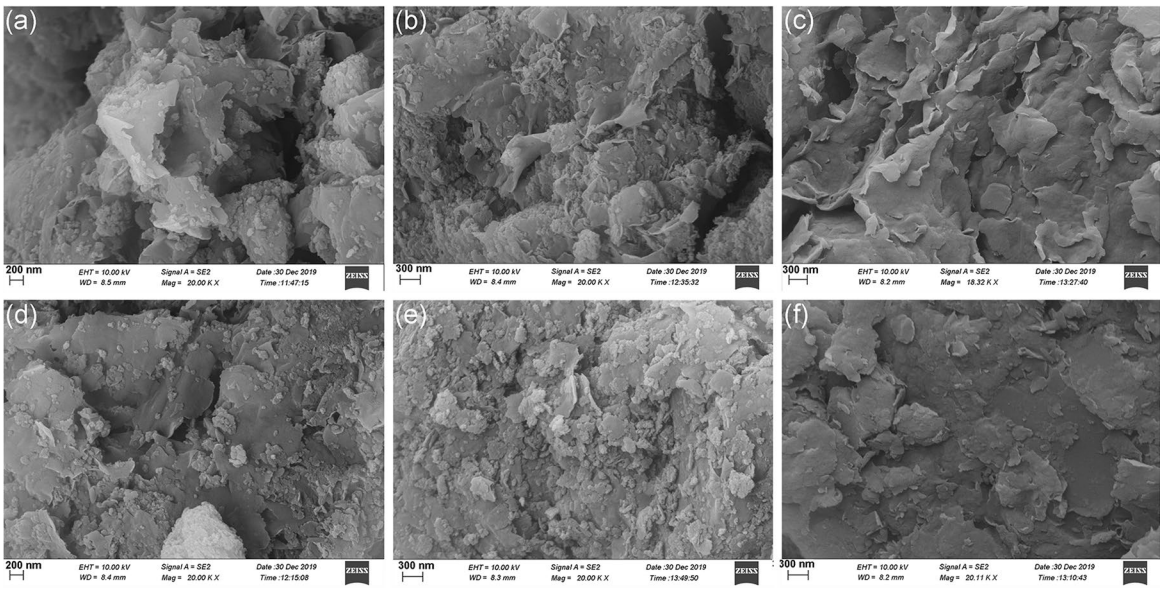

Fig. 5 SEM images of the bentonite samples before and after calcination at 600°C, **a** WH, **b** XY, **c** ST, **d** WH-600, **e** XY-600, and **f** ST-600

Table 6 Casting performance indicators of the bentonite samples

Sample	Swelling value (mL/3 g)	Consumption of methylene blue (g/100 g)	Consumption of methylene blue after calcination at 600°C (g/100 g)	Reusability (%)
WH	36.50	36.25	28.35	78.21
XY	19.17	48.50	4.60	9.48
ST	10.00	45.75	2.75	6.01

enhanced. Combined with the structural formula (Table 3) of the three samples, the amount of Al^{3+} substitution was largest in sample ST, moderate in sample XY, and smallest in sample WH. This showed that the thermal stability of bentonite (including its reusability) depended on the Q_m and increased with decreasing Q_m.

CONCLUSIONS

Samples from three mines (WH, XY, and ST) were all Ca-bentonite, and the main mineral impurities were quartz-type impurities. The Q_m of sample ST was greatest (0.725 e/huc), followed by sample XY (0.470 e/huc), and sample WH (0.354 e/huc). The dehydroxylation temperatures were 701, 684, and 630°C, respectively, which decreased with increasing Q_m. The XRD and FTIR data showed that after the three samples were calcined at 600°C for 60 min, the order of the structural integrity of montmorillonite was: WH > XY > ST. The reusability of sample WH was 78.21%, followed by sample XY with 9.48% and sample ST with 6.01%, which was proportional to the thermal stability of montmorillonite. The reusability of bentonite depended mainly on the thermal stability of montmorillonite, which, in turn, depends on Q_m. The reusability of bentonite increased with decreasing Q_m, therefore.

ACKNOWLEDGMENTS

This work was supported by the National Natural Fund of China [grant number 41972042,42072048] and the National Key R & D Program of China [grant number 2018YFC1802902].

Declarations

Conflict of Interest

On behalf of all authors, the corresponding author states that there is no conflict of interest.

https://doi.org/10.1007/s42860-021-00117-w Published online by Cambridge University Press

REFERENCES

Alver, B. E., & Gunal, A. (2016). Thermal, structural and ethylene adsorption properties of Ag-, Cu- and Fe-modified bentonite from Turkey. *Journal of Thermal Analysis and Calorimetry, 126*, 1533–1540.

Bala, P., Samantaray, B. K., & Srivastava, S. K. (2012). Dehydration transformation in Ca-montmorillonite. *Bulletin of Materials Science, 23*, 61–67.

Beňo, J., Vontorová, J., Matìjka, V., & Gál, K. (2015). Evaluation of the thermal resistance of selected bentonite binders. *Materiali in Tehnologije, 49*, 465–469.

Boeva, N. M., Bocharnikova, Y. I., Belousov, P. E., & Zhigarev, V. V. (2016). Determining the cation exchange capacity of montmorillonite by simultaneous thermal analysis method. *Russian Journal of Physical Chemistry A, 90*, 1525–1529.

Boylu, F. (2011). Optimization of foundry sand characteristics of soda-activated calcium bentonite. *Applied Clay Science, 52*, 104–108.

Caglar, B., Topcu, C., Coldur, F., Sarp, G., Caglar, S., Tabak, A., & Sahin, E. (2016). Structural, thermal, morphological and surface charge properties of dodecyltrimethylammonium-smectite composites. *Journal of Molecular Structure, 1105*, 70–79.

Chai, M., Li, C. X., Jiang, W., & Du, F. (2013). Effect of cations on thermal properties of montmorillonite. *Global Geology, 16*, 88–93.

Chen, T. X., Yuan, Y., Zhao, Y. L., Rao, F., & Song, S. X. (2018). Effect of layer charges on exfoliation of montmorillonite in aqueous solutions. *Colloids and Surfaces A – Physicochemical and Engineering Aspects, 548*, 92–97.

Finck, N., Schlegel, M. L., Dardenne, K., Adam, C., Kraft, S., Bauer, A., & Robert, J. L. (2019). Structural iron in smectites with different charge locations. *Physics and Chemistry of Minerals, 46*, 639–661.

Gauglitz, R., & Schwiete, H. E. (1964). Thermochemical investigations on montmorillonite with regards to type, grain size, and cation loading. *Berichte Deutsche Keramik Ges, 38*, 43–49.

Geng, G. F., & Liu, C. (2013). The application of bentonite on green sand molding. *China Foundry Machinery and Technology, 000*, 29–31.

Gong, Z. J., Liao, L. B., Lv, G. C., & Wang, X. Y. (2016). A simple method for physical purification of bentonite. *Applied Clay Science, 119*, 294–300.

Grim, R. E., & Rowland, R. A. (1942). Differential thermal analysis of clay minerals and other hydrous materials. *American Mineralogist, 27*, 746–761.

Hoang-Minh, T., Kasbohm, J., Nguyen-Thanh, L., Nga, P. T., Lai, L. T., Duong, N. T., Thanh, N. D., Thuyet, N. T. M., Anh, D. D., Pusch, R., Knutsson, S., & Mahlmann, R. F. (2019). Use of TEM-EDX for structural formula identification of clay minerals: A case study of Di Linh bentonite Vietnam. *Journal of Applied Crystallography, 52*, 133–147.

Holtzer, M., Bobrowski, A., & Żymankowska-Kumon, S. (2011). Temperature influence on structural changes of foundry bentonites. *Journal of Molecular Structure, 1004*, 102–108.

Jiang, X., Nie, J., Bian, L., Dong, F., Song, M., He, Y., He, H., Zheng, Z., Huo, T., Li, B., Belzile, N., Sun, S., & Zou, H. (2019). Competitive adsorption of uranyl and toxic trace metal ions at MFe_2O_4-montmorillonite (M = Mn, Fe, Zn Co, or Ni) interfaces. *Clays and Clay Minerals, 67*, 291–305.

Jordan, G., Eulenkamp, C., Calzada, E., Schillinger, B., Hoelzel, M., Gigler, A., Stanjek, H., & Schmahl, W. W. (2013). Quantitative in situ study of the dehydration of bentonite-bonded molding sands. *Clays and Clay Minerals, 61*, 133–140.

Kaufhold, S., Dohrmann, R., Ufer, K., & Meyer, F. M. (2003). Comparison of methods for the quantification of montmorillonite in bentonites. *Applied Clay Science, 22*, 145–151.

Kaufhold, S., Stucki, J. W., Finck, N., Steininger, R., Zimina, A., Dohrmann, R., Ufer, K., Pentrak, M., & Pentrakova, L. (2017). Tetrahedral charge and Fe content in dioctahedral smectites. *Clay Minerals, 52*, 51–65.

Koutsopoulou, E., Koutselas, I., Christidis, G. E., Papagiannopoulos, A., & Marantos, I. (2020). Effect of layer charge and charge distribution on the formation of chitosan-smectite bionanocomposites. *Applied Clay Science*. https://doi.org/10.1016/j.clay.2020.105583.

Liu, Y. L., Xu, B. Y., Qin, B., Tao, C. Z., Cao, L., Shen, Y. S., & Zhu, S. M. (2020). Novel nimow-clay hybrid catalyst for highly efficient hydrodesulfurization reaction. *Catalysis Communications*. https://doi.org/10.1016/j.catcom.2020.106086.

Magzoub, M. I., Nasser, M. S., Hussein, I. A., Benamor, A., Onaizi, S. A., Sultan, A. S., & Mahmoud, M. A. (2017). Effects of sodium carbonate addition, heat and agitation on swelling and rheological behavior of Ca-bentonite colloidal dispersions. *Applied Clay Science, 147*, 176–183.

Paluszkiewicz, C., Holtzer, M., & Bobrowski, A. (2008). FTIR analysis of bentonite in moulding sands. *Journal of Molecular Structure, 880*, 109–114.

Qiu, J., Li, G. Q., Liu, D. L., Jiang, S., Wang, G. F., Chen, P., Zhu, X. N., Yao, G., Liu, X. D., & Lyu, X. J. (2019a). Effect of layer charge density on hydration properties of montmorillonite: Molecular dynamics simulation and experimental study. *International Journal of Molecular Sciences, 20*, 3997–4013.

Qiu, J., Li, G. Q., Jiang, S., Liu, D. L., Chen, P., & Wang, G. F. (2019b). Effect of layer charge on adsorption properties of octadecyl trimethyl ammonium chloride by montmorillonite. *Science of Advanced Materials, 11*, 299–305.

Qiu, J., Zhang, Y. G., & Lv, X. J. (2007). Study on relation between layer charge and hydro-properties of montmorillonite. *Non-Metallic Mines, 30*, 15–17.

Rakhimova, N. R., Rakhimov, R. Z., Morozov, V. P., & Eskin, A. A. (2021). Calcined low-grade clays as sources for zeolite containing material. *Periodica Polytechnica-Civil Engineering, 65*, 204–214.

Sakizci, M., Alver, B. E., Alver, Ö., & Yörükoğullari, E. (2010). Spectroscopic and thermal studies of bentonites from Ünye, Turkey. *Journal of Molecular Structure, 969*, 187–191.

Sans, B. E., Guven, O., Esenli, F., & Celik, M. S. (2017). Contribution of cations and layer charges in the smectite structure on zeta potential of Ca-bentonites. *Applied Clay Science, 143*, 415–421.

Sarikaya, Y., Onal, M., Baran, B., & Alemdaroglu, T. (2000). The effect of thermal treatment on some of the physicochemical properties of a bentonite. *Clays and Clay Minerals, 48*, 557–562.

Schnetzer, F., Thissen, P., Giraudo, N., & Emmerich, K. (2016). Unraveling the coupled processes of (De) hydration and structural changes in Na^+-saturated montmorillonite. *Journal of Physical Chemistry C, 120*, 15282–15287.

Sun, H. J., Peng, T. J., Liu, B., & Xian, H. Y. (2015). Effects of montmorillonite on phase transition and size of TiO_2 nanoparticles in TiO_2/montmorillonite nanocomposites. *Applied Clay Science, 114*, 440–446.

Sun, H. J., Peng, T. J., & Liu, Y. (2007). Measurement and mechanism of layer charge of phyllosilicate with expansive layers. *Acta Mineralogica Sinica, 27*, 19–24.

Ufer, K., Stanjek, H., Roth, G., Dohrmann, R., Kleeberg, R., & Kaufhold, S. (2008). Quantitative phase analysis of bentonites by the rietveld method. *Clays and Clay Minerals, 56*, 272–282.

Wolters, F., & Emmerich, K. (2007). Thermal reactions of smectites-Relation of dehydroxylation temperature to octahedral structure. *Thermochimica Acta, 462*, 80–88.

Wu, P., Wu, H., & Li, R. (2005). The microstructural study of thermal treatment montmorillonite from Heping, China. *Spectrochimica Acta. Part A, Molecular and Biomolecular Spectroscopy, 61*, 3020–3025.

Wu, P. X., Zhang, H. F., Wang, F. Y., Guo, J. G., & Zhao, W. X. (1999). The SEM study on the montmorillonite and its thermal treatment products. *Mineralogy and Petrology, 19*, 21–25.

Yang, Y. F., Nair, A. K. N., & Sun, S. Y. (2019). Layer charge effects on adsorption and diffusion of water and ions in interlayers and on external surfaces of montmorillonite. *ACS Earth and Space Chemistry, 3*, 2635–2645.

Yang, Y., Yao, H., & Chen, S. (2006). Characteristics of microcosmic structure of guangxi expansive soil. *Rock and Soil Mechanics, 27*, 155–158.

Zhu, T. T., Zhou, C. H., Kabwe, F. B., Wu, Q. Q., Li, C. S., & Zhang, J. R. (2019). Exfoliation of montmorillonite and related properties of clay/polymer nanocomposites. *Applied Clay Science, 169*, 48–66.

Żymankowska-Kumon, S., Holtzer, M., Olejnik, E., & Bobrowski, A. (2012). Influence of the changes of the structure of foundry bentonites on their binding properties. *Materials Science, 18*, 57–61.

(Received 5 November 2020; revised 12 February 2021; AE: Runliang Zhu)